



Published in final edited form as:

Kotadiya, N. B., Lu, H., Mondal, A., Ie, Y., Andrienko, D., Blom, P. W. M., et al. (2018). Universal strategy for Ohmic hole injection into organic semiconductors with high ionization energies. *Nature Materials*, 17(4), 329-334. doi:10.1038/s41563-018-0022-8.

Universal strategy for Ohmic hole injection into organic semiconductors with high ionization energies

Kotadiya, N. B., Lu, H., Mondal, A., Ie, Y., Andrienko, D., Blom, P. W. M., Wetzelaer, G.-J. A. H.

This article may be used for non-commercial purposes in accordance with publisher's Terms and Conditions for Self-Archiving.

1 **Universal strategy for ohmic hole injection into organic semiconductors with high ionization**
2 **energies**

3
4 Naresh B. Kotadiya,¹ Hao Lu,¹ Anirban Mondal,¹ Yutaka Ie,^{1,2} Denis Andrienko,¹ Paul W. M. Blom,¹
5 and Gert-Jan A. H. Wetzelaer¹

6
7 ¹*Max Planck Institute for Polymer Research, Ackermannweg 10, 55128 Mainz, Germany*

8 ²*The Institute of Scientific and Industrial Research (ISIR), Osaka University, 8-1 Mihogaoka, Ibaraki,*
9 *Osaka 567-0047, Japan*

10
11 Barrier-free (ohmic) contacts are a key requirement for efficient organic optoelectronic devices, such
12 as organic light-emitting diodes, solar cells, and field-effect transistors. Here, we propose a simple
13 and robust way of forming an ohmic hole contact on organic semiconductors with a high ionization
14 energy (IE). The injected hole current from high work function metal-oxide electrodes is improved by
15 more than an order of magnitude by using an interlayer for which the sole requirement is that it has a
16 higher IE than the organic semiconductor. Insertion of the interlayer results in electrostatic decoupling
17 of the electrode from the semiconductor and realignment of the Fermi level with the IE of the organic
18 semiconductor. The ohmic-contact formation is illustrated for a number of material combinations and
19 solves the problem of hole injection into organic semiconductors with a high IE of up to 6 eV.
20

21 One of the most important requirements for efficient organic-semiconductor devices is the
22 establishment of ohmic contacts for holes and electrons. To create an ohmic contact for holes, the
23 electrode work function should match the ionization energy (IE) of the organic semiconductor. In
24 organic light-emitting diodes (OLEDs), materials with an IE as high as 6 eV are commonly used as
25 hosts and emitters [1,2]. However, typical electrodes used in organic devices, such as indium-tin
26 oxide (ITO) and PEDOT:PSS have work functions close to 5.0 eV [3,4], which give rise to large
27 injection barriers. Since the injected current depends exponentially on the injection barrier [5], it is
28 vital to find hole-injecting electrodes with a considerably higher work function. For example,
29 chlorinated ITO can reach work functions of up to 6.1 eV [4]. However, a sizable contact barrier of
30 about 0.5 eV was still observed when the electrode was put in contact with the popular 4,4'-bis(N-
31 carbazolyl)biphenyl (CBP) organic host material, which has an IE of 6.0 eV [4].

32 An alternative method to obtain ohmic contacts is the use of a p-type doped hole-injection
33 layer. The resulting strong band bending in the doped layer then allows for injection via tunneling.
34 However, a typical p-type dopant such as F6TCNNQ has an electron affinity of ~5.6 eV [6], such that
35 doping will not be effective for semiconductors with an IE larger than 5.6 eV. Very recently, a
36 strategy was reported to achieve doped organic-semiconductor films with work functions up to 5.8 eV
37 [7]. Using a doped polymer film as a hole-injection layer, they showed that hole injection into a
38 conjugated polymer with an IE of 5.8 eV was almost as efficient as the injection from a thermally-
39 evaporated MoO₃ reference.

40 MoO₃ is widely used as a hole contact in organic solar cells and OLEDs, owing to its
41 extremely high work function of 6.9 eV [8]. MoO₃ is an n-type semiconductor, with an electron
42 affinity of 6.7 eV and an ionization energy of 9.7 eV [8]. Because of its high electron affinity, MoO₃
43 can be used as a p-type dopant in CBP [9]. Since transition-metal oxides like MoO₃, V₂O₅, and WO₃
44 possess the combined quality of optical transparency and a very high work function of 6.7-7.0 eV,
45 they seem to be ideal hole contacts, and are frequently applied in organic-semiconductor devices [10].

46 Here, we demonstrate that despite their high work function, transition-metal oxides give rise
47 to a considerable injection barrier when put into contact with organic semiconductors. We present a
48 strategy to completely eliminate this injection barrier by electrostatic decoupling of the electrode from

49 the organic semiconductor, enabling the formation of an ohmic contact with organic semiconductors
50 with an IE as high as 6 eV.

51 A direct way to investigate the hole-injection capability of an electrode into an organic
52 semiconductor is to fabricate so-called hole-only devices. In such a device, an organic-semiconductor
53 layer is sandwiched between two high work function electrodes, to prevent the injection of electrons.
54 When applying a voltage across the device, the measured current is carried exclusively by holes, and
55 the magnitude of the current is a measure of the hole-injection capabilities of one of the two
56 electrodes, depending on the sign of the applied voltage. Since the current depends exponentially on
57 the injection barrier [5], the measured current is very sensitive to changes in the barrier height. When
58 the barrier height approaches zero, the contact can be regarded as ohmic, and a transition from an
59 injection-limited current into a space-charge-limited current will occur, which is governed by the
60 charge-carrier mobility of the organic semiconductor [11,12].

61 In Fig. 1(a), the current through a hole-only device of the organic semiconductor Spiro-TAD
62 is displayed. Here, Spiro-TAD is sandwiched between a PEDOT:PSS bottom electrode and a
63 MoO₃(10 nm)/Al top electrode. Since Spiro-TAD has a moderate IE of 5.3 eV [13], hole injection
64 from MoO₃ with a high work function of 6.9 eV is expected to be efficient. Surprisingly, as can be
65 seen in Fig. 1, the current injected from MoO₃ (forward bias) is even lower than the current injected
66 from PEDOT:PSS (reverse bias). Apparently, a hole-injection barrier at the Spiro-TAD/MoO₃
67 interface is present that lowers the injected current. As also can be observed in Fig. 1(a), the hole
68 injection is improved considerably by inserting a 5 nm layer of TCTA between Spiro-TAD and MoO₃.
69 By using the TCTA interlayer, the current injected from MoO₃ increases by over an order of
70 magnitude, up to a factor of 30. This is a counterintuitive result, since TCTA has a higher IE (5.7 eV
71 [14]) than Spiro-TAD, which usually aggravates hole-injection problems.

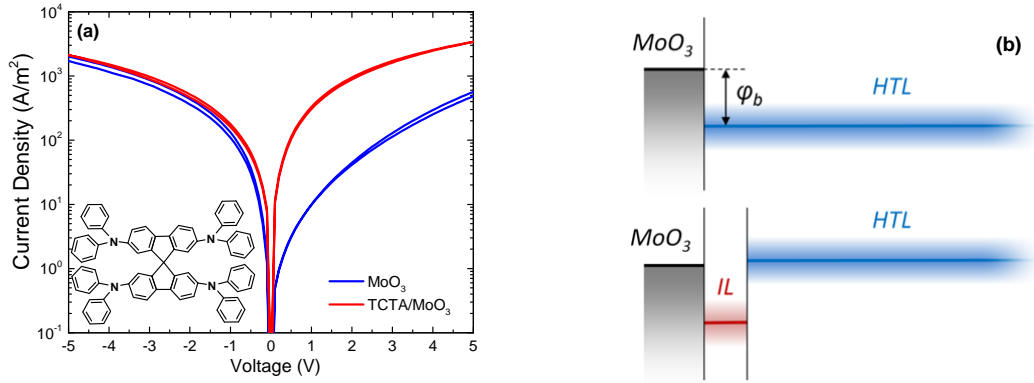
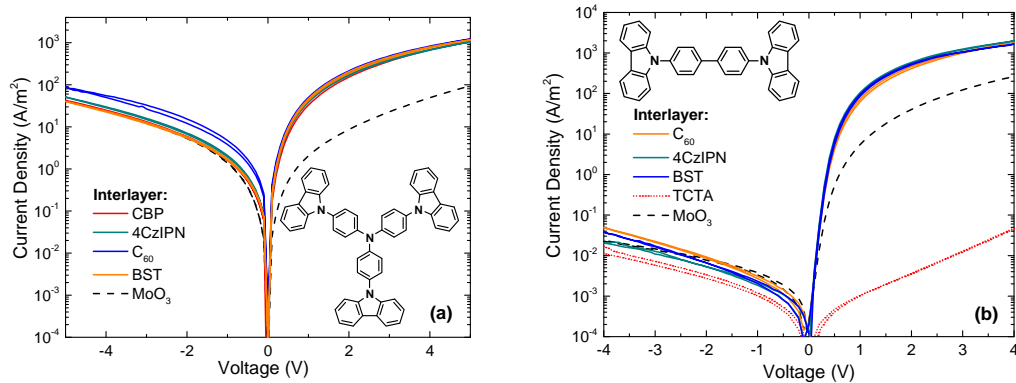


Figure 1. Hole-injection enhancement in Spiro-TAD. (a) Current density-voltage characteristics of a PEDOT:PSS/Spiro-TAD/MoO₃ hole-only device with and without a TCTA (5 nm) interlayer between the Spiro-TAD (163 nm) transport layer and MoO₃. Negative bias corresponds to hole injection from the PEDOT:PSS, positive bias to hole injection from MoO₃. The inset shows the molecular structure of Spiro-TAD. (b) Schematic energy-band diagram showing the *effective* injection barrier (ϕ_b) between MoO₃ and the hole-transport layer (HTL). Introducing an interlayer (IL) with a higher IE realigns the Fermi level with the IE of the HTL.

To demonstrate that the injection barrier at the organic/MoO₃ interface is not an exclusive property of Spiro-TAD, Fig. 2 shows that a similar hole-injection barrier exists between MoO₃ and the organic small molecules TCTA and CBP, which have an IE of 5.7 eV and 6.0 eV, respectively [14]. For both materials, the current injected from MoO₃ is improved by more than an order of magnitude by inserting a 5 nm interlayer of an organic semiconductor with a higher IE. In fact, independent of the material used for the interlayer, the current is universally improved to the same magnitude and voltage dependence, even for a material with a high IE like CBP.



88 **Figure 2. Hole-injection enhancement with different interlayers.** Current density-voltage characteristics of TCTA (a; 239
 89 nm) and CBP (b; 215 nm) hole-only devices with different interlayers. The hole current injected from MoO₃ (positive bias)
 90 improves to the same level whenever the IE of the interlayer is larger than the IE of the transport layer. For the case of CBP
 91 with a TCTA interlayer (b; red dotted line), the offset in IE is negative, resulting in a large reduction of the injected current.
 92 The insets in (a) and (b) show the molecular structures of TCTA and CBP, respectively.

94 Identical improvements were obtained for the high work function metal oxides WO₃ and
 95 V₂O₅, as shown in the Supplementary Information (SI). It is also demonstrated in the SI that equally
 96 high currents are obtained when applying the interlayer strategy to the bottom electrode. MoO₃ can
 97 diffuse into the organic layers when it is deposited on top of organic semiconductors, while a non-
 98 intermixed interface is obtained when organic layers are deposited on top of MoO₃ [14]. Despite
 99 deposition-order inversion, improvements in hole injection are identical, ruling out diffusion of MoO₃
 100 as the mechanism for the observed hole-injection enhancement.

101 Figure 2(b) also shows how problematic hole injection into CBP is with conventional hole-
 102 injection layers like PEDOT:PSS (reverse bias). The current in reverse bias is around 5 orders of
 103 magnitude lower than the current injected in forward bias, which is the result of the hole-injection
 104 barrier arising from the mismatch between the work function of PEDOT:PSS (5.0-5.2 eV) and the IE
 105 of CBP.

107 **Table 1. Ionization energies and hole mobilities of materials used in this work.** IEs are obtained with ultraviolet
 108 photoelectron spectroscopy. Mobilities are obtained from space-charge-limited currents (Fig. 3), which are compared to
 109 time-of-flight measurements from literature.

Material	IE (eV)	SCLC mobility (m ² /Vs)	TOF mobility (m ² /Vs)
2-TNATA	5.0 [17]	5×10^{-9}	3×10^{-9} [25]
Spiro-TAD	5.3 [13]	5×10^{-8}	3×10^{-8} [26]
TCTA	5.7 [14]	1.4×10^{-8}	2×10^{-8} [27]
CBP	6.0 [14,17]	7×10^{-8}	5×10^{-8} [28]
4CzIPN	6.1 [23]	-	-

C ₆₀	6.4 [14]	-	-
BST	7.0 [this work]	-	-

From the results on Spiro-TAD (see SI), TCTA, and CBP, it is inferred that hole injection is improved universally when the offset between the IE of the interlayer and transport material is larger than 0.2-0.3 eV. Conversely, when the IE of the interlayer is lower than the IE of the transport material, resulting in an energetic staircase, the injected current drops by several orders of magnitude. This is demonstrated in Fig. 2(b) for the case of a TCTA interlayer on CBP, for which the IE offset has a negative value of -0.3 eV. It appears that there is no maximum to the value of the offset: the improvement in injection is observed for offsets of more than 1 eV.

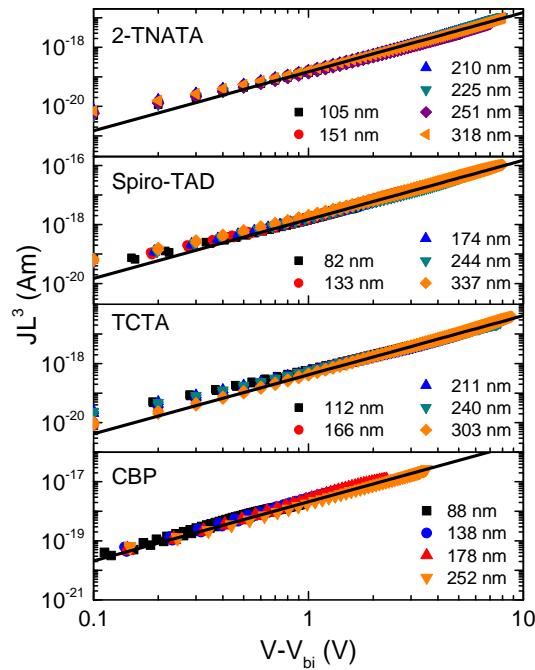
The fact that the current for all investigated organic semiconductors reaches a maximum magnitude independent of the used interlayer strongly suggests that the current is no longer injection limited. This would imply that the use of an interlayer results in the formation of an ohmic contact. To validate this hypothesis, it should be verified that the injected currents are space-charge limited. A space-charge-limited current is the maximum electrostatically-allowed current that can pass through the organic-semiconductor layer. A trap-free space-charge-limited current is characterized by the Mott-Gurney square law [15]

$$J = \frac{9}{8} \varepsilon \mu \frac{(V - V_{bi})^2}{L^3} \quad (1)$$

where J is the current density, ε is the permittivity, μ is the charge-carrier mobility, V is the applied voltage, V_{bi} is the built-in voltage due to asymmetric work functions of the electrodes, and L is the layer thickness.

To test if the injected hole currents are indeed space-charge limited, the current needs to fulfill two important criteria: i) the current depends quadratically on voltage, and ii) the current scales inversely with layer thickness to the third power. The layer-thickness dependence can be directly confirmed by plotting JL^3 against voltage. In case of a space-charge-limited current, the measured current for a range of layer thicknesses will collapse onto a single curve. This is indeed the case, as shown in Fig. 3. For all tested organic semiconductors, the L^{-3} layer-thickness dependence is fulfilled.

135 In addition, the experimental current depends on the square of voltage, proving that the injected
 136 current is indeed space-charge limited. The establishment of a space-charge-limited current after
 137 insertion of the interlayer confirms the formation of an ohmic hole contact. These results therefore
 138 demonstrate the formation of a truly ohmic contact on organic semiconductors with an IE of up to 6
 139 eV.



140
 141 **Figure 3. Space-charge-limited hole currents in four different materials.** TCTA was used as an interlayer for 2-TNATA
 142 and Spiro-TAD transport layers, whereas CBP and BST interlayers were used for TCTA and CBP transport layers,
 143 respectively. For all materials, JL^3 is plotted for a range of layer thicknesses against voltage, corrected for the built-in voltage
 144 and the electrode series resistance. The lines represent fits with Eq. (1), from which the hole mobility is extracted.

145
 146 A space-charge-limited current can also be used to determine the charge-carrier mobility of
 147 organic semiconductors, as is evident from Eq. (1). The mobilities determined for 2-TNATA, Spiro-
 148 TAD, TCTA, and CBP are in excellent agreement with the low-field values measured by the time-of-
 149 flight technique, see Table 1. It is known that the time-of-flight technique can overestimate the
 150 mobility, especially when charge trapping is present [16]. However, the fact the mobilities from

151 space-charge-limited currents are close to the time-of-flight values shows that i) hole injection is
152 indeed maximized (ohmic contact) by using an interlayer and ii) the current is not decreased by
153 trapping effects. Interestingly, as a result of the high injection efficiency of the interlayer-enhanced
154 contact, the space-charge conductivity of an 88 nm undoped CBP layer amounts to 2.5×10^{-6} S/cm,
155 which even surpasses the conductivity of highly p-doped CBP with 22.1 mol% of MoO₃ (1×10^{-6}
156 S/cm) [9].

157 Knowing the hole mobilities from the measured space-charge-limited currents, we can now
158 determine the injection barriers from the injection-limited currents observed for transition-metal oxide
159 electrodes (MoO₃, V₂O₅, and WO₃) without interlayer. For all investigated organic semiconductors
160 and metal oxides, an injection barrier of 0.39 ± 0.03 eV was determined (see SI), independent of the
161 IE of the organic semiconductor. Interestingly, a universal energy-alignment behavior between metal
162 oxides and organic semiconductors has been reported, where a general 0.3 eV offset was observed
163 between the work function of the oxide and the IE of the organic semiconductor [17]. These
164 ultraviolet photoelectron spectroscopy (UPS) measurements suggest that the energy offset is
165 manifested as an injection barrier.

166 To unravel the mechanism of the ohmic-contact formation, the energy-level alignment in the
167 presence of an interlayer was investigated. For this purpose, UPS measurements were performed
168 layer-by-layer on a representative MoO₃/TCTA/2-TNATA structure, which has an IE offset of 0.7 eV
169 between the TCTA interlayer and 2-TNATA. Figure 4 shows the measured IE as a function of layer
170 thickness. At a TCTA coverage of 1 nm, the Fermi level of MoO₃ is pinned at 0.38 eV below the IE of
171 TCTA, in line with the universal offset in the pinning regime [17]. With increasing TCTA thickness,
172 the IE separates further from the Fermi level to 0.6 eV at 5 nm, which abruptly reduces to 0.16 eV
173 upon 2-TNATA coverage, because of the IE offset between TCTA (5.7 eV) and 2-TNATA (5.0 eV).
174 This shows that, near the interface, the IE of 2-TNATA aligns with the Fermi level, which is the
175 required condition for the formation of an ohmic contact. The energy offset of 0.16 eV is substantially
176 smaller than the universal offset of 0.3 eV in the monolayer regime as previously observed [17],
177 explaining the improved injection with the help of the interlayer.

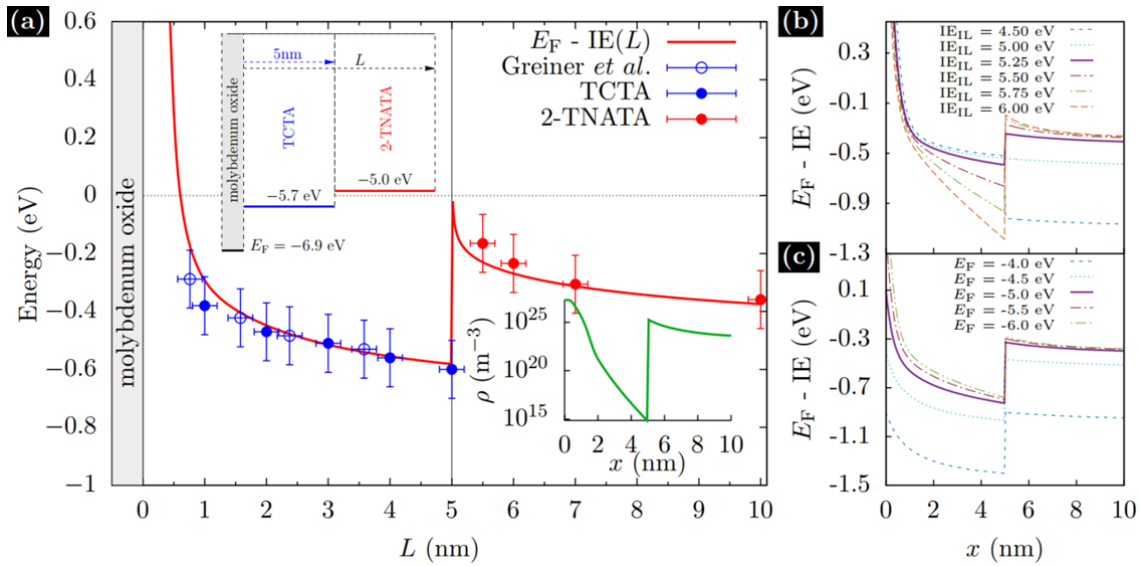


Figure 4. Experimental and calculated IE profiles across interlayer/hole-transport layer structures. (a) IE onset with respect to the Fermi level obtained by UPS layer by layer across a MoO₃/TCTA(5 nm)/2-TNATA(5 nm) structure (closed symbols), augmented with data of the universal IE profile of organic semiconductors on metal oxides [17] (open symbols). The calculated IE position at the layer surface (red line), corresponding to the UPS measurements, is obtained by evaluating the band bending at $x = L$ for different L . The top inset shows the energy levels of the separate materials and the bottom inset shows the calculated charge density across the layers. (b) Simulated band diagrams (IE as a function of position x across the layers) for different interlayer IEs, using a work function of 6.9 eV and a HTL IE of 5.0 eV. (c) Band diagrams for different work functions, with an IE of 5.5 eV for the interlayer and 5.0 eV for the HTL

To understand the band alignment as well as the (universal) barrier reduction, the IE profile was calculated by solving Poisson’s equation, as described in the SI. The Poisson equation relates charge density to electrostatic potential, both of which depend on the relative alignment of the oxide Fermi level with respect to the density of states (DOS) of the organic semiconductor [18-20]. As shown in Fig. 4, within the first nanometer, a strong band bending is observed as a result of charge transfer between MoO₃ and TCTA to establish thermodynamic equilibrium across the interface. In the monolayer regime, the Fermi level is (universally [14,17]) pinned at 0.3-0.4 eV below the IE of TCTA, which could be reproduced by considering a broadened DOS near the metal oxide, as suggested in previous publications [19,21,22]. Effectively, the Fermi level is pinned to the deeper states in the broadened interface DOS, from which charges have to escape to the narrower bulk DOS, leading to an injection barrier. The band bending for increasing layer thickness is well described by

199 including a Coulomb image potential due to differences in dielectric constants between MoO₃ and the
200 organic semiconductor (see SI). We suggest DOS broadening at the interface and the attractive image
201 potential to be the reason for the observed injection barriers at the metal-oxide contact.

202 At the TCTA/2-TNATA interface, the calculations support alignment of the IE of 2-TNATA
203 with the Fermi level, which is accompanied by the presence of a high hole density (inset Fig. 4). The
204 experimental IE profile of the 2-TNATA layer is consistently described by using a Gaussian DOS
205 width of 0.1 eV, without additional broadening. This disorder value is also consistent with molecular
206 dynamics simulations of layered structures and evaluated energetic disorder in the organic films using
207 polarizable force fields, showing no distinct DOS broadening at the organic/organic interfaces, as
208 described in the SI. In short, the interlayer realigns the Fermi level with the IE of the organic
209 semiconductor, negating the barrier formation due to DOS broadening and the image potential by
210 effectively decoupling the electrode and semiconductor electrostatically.

211 With the developed model, we can now explore the limiting cases for the formation of an
212 ohmic contact by simulating band diagrams. By varying the interlayer IE in Fig. 4(b), it is found that
213 the IE in the HTL is close to the Fermi level for an interlayer offset of at least ~0.3 eV, with larger
214 offsets having no effect on the energetic position of the HTL, as confirmed experimentally in Fig. 2
215 by the identical currents obtained for different interlayers with varying offsets. In a similar fashion,
216 electrode work functions that are equal or higher than the IE of the HTL are required [Fig. 4(c)],
217 which is the case in our injection experiments with the high work function metal oxides MoO₃, V₂O₅,
218 and WO₃.

219 The UPS measurements and simulations indicate a high hole density at the organic/organic
220 interface [inset Fig. 4(a)], which plays the role of a virtual ohmic hole contact, spatially separated
221 from the electrode by the interlayer. However, charges still have to pass through the interlayer to
222 contribute to the current. Considering the measured space-charge-limited currents with mobilities that
223 are close to the time-of-flight values, even for thin transport layers of less than 100 nm, it can be
224 concluded that the interlayer does not add a significant resistance. In addition, as can be seen from the
225 experimental currents in reverse bias where the current is injected from the PEDOT:PSS electrode, the
226 presence of the interlayer does not reduce the current, even for large IE offsets between the transport

227 material and the interlayer, which normally imposes a hole-extraction barrier. This indicates that the
228 interlayer is virtually transparent for holes.

229 Since the measured current is the same regardless of the interlayer material, it appears that the
230 transport properties of different interlayers do not affect the injected current. However, at interlayer
231 thicknesses above 5 nm, the current is reduced and depends on the interlayer material (see SI),
232 suggesting that transport through and injection into the interlayer becomes a limiting factor. This
233 supports a scenario in which charges tunnel through the electrostatic barrier of the interlayer to the
234 second layer. For thick interlayers, the charge density decreases and the tunneling rates become
235 negligible, thus explaining that the optimal interlayer thickness is below 5 nm. On the other hand, the
236 optimum thickness of 3-5 nm helps to decrease the barrier due to the attractive image potential near
237 the electrode interface, which is strongly reduced at these length scales.

238 As an ultimate proof, we demonstrate our hole injection strategy in a light-emitting diode
239 based on the electron-transport material TPBi. Because of its high ionization energy of 6.3 eV, TPBi
240 is frequently used as a hole-blocking material in OLEDs [23,24]. Here, we use TPBi in a UV-emitting
241 diode, consisting of TPBi sandwiched between a MoO₃ anode and a Ba cathode. As demonstrated in
242 Fig. 5, adding an additional C₆₀ interlayer between MoO₃ and TPBi results in a three orders of
243 magnitude increased light output and efficiency. The increased light output is a direct consequence of
244 the enhanced hole injection, showing that it is possible to directly inject holes even in materials that
245 are normally used for hole-blocking purposes. Since TPBi is an electron transporter [24], the current
246 through the OLED is mainly carried by electrons and does not increase by improving the hole contact.
247 However, the J - V characteristics are shifted by 0.6 V along the voltage axis, which is the result of an
248 increased built-in voltage due to the reduced barrier on the anode side, which in turn enhances the
249 hole injection and light output.

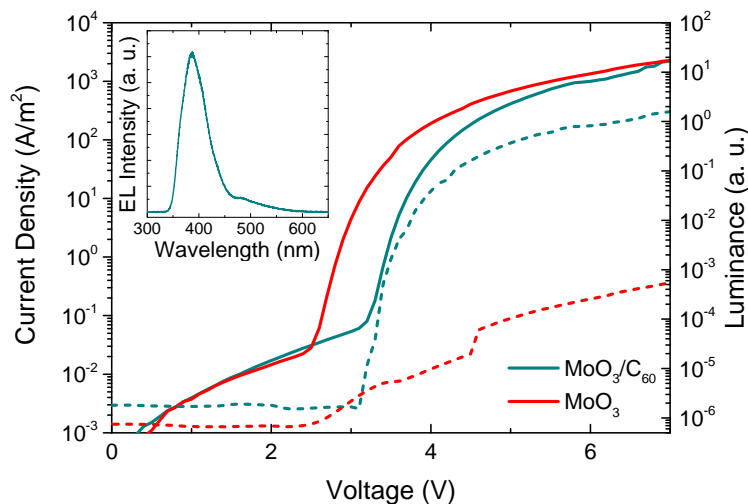


Figure 5. UV-emitting TPBi OLEDs. Current density-voltage (solid lines) and luminance-voltage (dashed lines) characteristics of OLEDs with a MoO₃/[C₆₀(4 nm)]/TPBi(58 nm)/Ba/Al structure, with and without a C₆₀ interlayer. The inset shows the electroluminescence spectrum corresponding to TPBi emission, with an onset at 340 nm and a maximum at 385 nm.

In conclusion, we present a universal strategy for achieving ohmic hole contacts on organic semiconductors with a high IE. In particular, the injected hole current is consistently improved by over an order of magnitude as compared to high work function transition-metal oxide electrodes. The barrier reduction is rationalized by electrostatic decoupling of the electrode from the organic semiconductor with an interlayer. This interlayer strongly reduces the effect of the attractive image potential near the electrode interface, and eliminates the density-of-states broadening present at the organic/electrode interface, while restoring Fermi-level alignment. As a proof of principle, we illustrate that the interlayer-enhanced contact can be used in a UV-emitting diode, providing direct hole injection into the hole-blocking material TPBi. The presented efficient hole injection into organic semiconductors with ionization energies beyond 6 eV extends the range of materials available for OLEDs and organic photovoltaic devices, which otherwise would suffer from high contact barriers.

268

269 Data availability

270 Experimental data are available from the corresponding author upon reasonable request.

271

272 Acknowledgments

273 The authors thank Christian Bauer, Frank Keller, and Hans-Jürgen Guttman for technical support.
274 This project has received funding from the European Union Horizon 2020 research and innovation
275 programme under Grant Agreement No. 646176 (EXTMOS). D.A. thanks the BMBF grant InterPhase
276 (FKZ 13N13661) and the European Union Horizon 2020 research and innovation program
277 “Widening materials models” under Grant Agreement No. 646259 (MOSTOPHOS).

278

279 Author contributions

280 G.A.H.W. proposed and supervised the project. N.B.K. carried out sample preparation and electrical
281 measurements. H.L. performed the UPS measurements. D.A. and A.M. performed molecular-
282 dynamics and energy-alignment simulations. Y.I. synthesized and purified 4CzIPN. G.A.H.W.,
283 N.B.K., and P.W.M.B. analysed the experimental data. G.A.H.W. wrote the manuscript with input
284 from D.A. and P.W.M.B.

285

286 Competing financial interests

287 The authors declare no competing financial interests.

288

289
290
291
292
293
294
295
296
297
298
299
300
301
302
303
304
305
306
307
308
309
310
311
312
313
314
315
316
317
318
319
320
321
322
323
324
325**References**

- [1] Tao, Y., Yang, C. & Qin, J. Organic host materials for phosphorescent organic light-emitting diodes. *Chem. Soc. Rev.* **40**, 2943-2970 (2011).
- [2] Wong, M. Y. & Zysman-Colman, E. Purely organic thermally activated delayed fluorescence materials for organic light-emitting diodes. *Adv. Mater.* **29**, 1605444 (2017).
- [3] Koch, N. & Vollmer, A. Electrode-molecular semiconductor contacts: Work-function-dependent hole injection barriers versus Fermi-level pinning. *Appl. Phys. Lett.* **89**, 162107 (2006).
- [4] Helander, M. G., Wang, Z. B., Qiu, J., Greiner, M. T., Puzzo, D. P., Liu, Z. W. & Lu, Z. H. Chlorinated indium tin oxide electrodes with high work function for organic device compatibility, *Science* **332**, 944-947 (2011).
- [5] Simmons, J.G. Richardson-Schottky effect in solids. *Phys. Rev. Lett.* **15**, 967-968 (1965).
- [6] Méndez, H., Heimel, G., Winkler, S., Frisch, J., Opitz, A., Sauer, K., Wegner, B., Oehzelt, M., Röthel, C., Duhamel, S., Többsens, D., Koch, N. & Salzmann, I. Charge-transfer crystallites as molecular electrical dopants. *Nat. Commun.* **6**, 8560 (2015).
- [7] Tang, C. G., Ang, M. C. Y., Choo, K.-K., Keerthi, V., Tan, J.-K., Syafiqah, M. N., Kugler, T., Burroughes, J. H., Png, R.-Q., Chua, L.-L. & Ho, P. K. H. Doped polymer semiconductors with ultrahigh and ultralow work functions for ohmic contacts. *Nature* **539**, 536-540 (2016).
- [8] Kröger, M., Hamwi, S., Meyer, J., Riedl, T., Kowalsky, W. & Kahn, A. Role of the deep-lying electronic states of MoO₃ in the enhancement of hole-injection in organic thin films. *Appl. Phys. Lett.* **95**, 123301 (2009).
- [9] Kröger, M., Hamwi, S., Meyer, J., Riedl, T., Kowalsky, W. & Kahn, A. P-type doping of organic wide band gap materials by transition metal oxides: A case-study on Molybdenum trioxide. *Org. Electron.* **10**, 932-938 (2009).
- [10] Meyer, J., Hamwi, S., Kröger, M., Kowalsky, W., Riedl, T. & Kahn, A. Transition Metal Oxides for Organic Electronics: Energetics, Device Physics and Applications. *Adv. Mater.* **24**, 5408-5427 (2012).
- [11] Blom, P. W. M., de Jong, M. J. M. & Vleggaar, J. J. M. Electron and hole transport in poly(p-phenylene vinylene) devices. *Appl. Phys. Lett.* **68**, 3308-3310 (1996).
- [12] Davids, P. S., Campbell, I. H. & Smith, D. L. Device model for single carrier organic diodes. *J. Appl. Phys.* **82**, 6319-6325 (1997).
- [13] Belisle, R. A., Jain, P., Prasanna, R., Leijtens, T. & McGehee, M. D. Minimal effect of the hole-transport material ionization potential on the open-circuit voltage of perovskite solar cells. *ACS Energy Lett.* **1**, 556-560 (2016).
- [14] White, R. T., Thibau, E. S. & Lu, Z.-H. Interface structure of MoO₃ on organic semiconductors. *Sci. Rep.* **6**, 21109 (2016).

- 326 [15] Mott, N. F. & Gurney, R. W. *Electronic Processes in Ionic Crystals* (Oxford University Press,
327 London, 1940).
- 328 [16] Li, C., Duan, L., Li, H. & Qiu, Y. Universal trap effect in carrier transport of disordered
329 organic semiconductors: Transition from shallow trapping to deep trapping. *J. Phys. Chem. C*
330 **118**, 10651-10660 (2014).
- 331 [17] Greiner, M. T., Helander, M. G., Tang, W.-M., Wang, Z.-B., Qiu, J. & Lu, Z.-H. Universal
332 energy-level alignment of molecules on metal oxides. *Nat. Mater.* **11**, 76-81 (2012).
- 333 [18] Blakesley, J. C. & Greenham, N. C. Charge transfer at polymer-electrode interfaces: The
334 effect of energetic disorder and thermal injection on band bending and open-circuit voltage. *J.*
335 *Appl. Phys.* **106**, 034507 (2009).
- 336 [19] Oehzelt, M., Koch, N. & Heimel, G. Organic semiconductor density of states controls the
337 energy level alignment at electrode interfaces. *Nat. Comm.* **5**, 4174 (2014).
- 338 [20] Oehzelt, M., Akaike, K., Koch, N. & Heimel, G. Energy-level alignment at organic
339 heterointerfaces. *Sci. Adv.* **1**, e1501127 (2015).
- 340 [21] Baldo, M. A., & Forrest, S. R. Interface-limited injection in amorphous organic
341 semiconductors. *Phys. Rev. B* **64**, 085201 (2001).
- 342 [22] Limketkai, B. N. & Baldo, M. A. Charge injection into cathode-doped amorphous organic
343 semiconductors. *Phys. Rev. B* **71**, 085207 (2005).
- 344 [23] Seino, Y., Inomata, S., Sasabe, H., Pu, Y.-J. & Kido, J. High-performance green OLEDs using
345 thermally activated delayed fluorescence with a power efficiency of over 100 lm W⁻¹. *Adv.*
346 *Mater.* **28**, 2638-2643 (2016).
- 347 [24] Hung, W.-Y., Ke, T.-H., Lin, Y.-T., Wu, C.-C., Hung, T.-H., Chao, T.-C., Wong, K.-T. &
348 Wu, C.-I. Employing ambipolar oligofluorene as the charge-generation layer in time-of-flight
349 mobility measurements of organic thin films. *Appl. Phys. Lett.* **88**, 064102 (2006).
- 350 [25] Tse, S. C., Kwok, K. C. & So, S. K. Electron transport in naphthylamine-based organic
351 compounds. *Appl. Phys. Lett.* **89**, 262102 (2006).
- 352 [26] Bach, U., De Cloedt, K., Spreitzer, H. & Grätzel, M. Characterization of hole transport in a
353 new class of spiro-linked oligotriphenylamine compounds. *Adv. Mater.* **12**, 1060-1063 (2000).
- 354 [27] Noh, S., Suman, C. K., Hong, Y. & Lee, C. Carrier conduction mechanism for
355 phosphorescent material doped organic semiconductor. *J. Appl. Phys.* **105**, 033709 (2009).
- 356 [28] Matusue, N., Suzuki, Y. & Naito, H. Charge carrier transport in neat thin films of
357 phosphorescent iridium complexes. *Jpn. J. Appl. Phys.* **44**, 3691-3694 (2005).
- 358

359 **Methods**

360 *Materials:* 4CzIPN was synthesized according to the procedure described in literature [29] and
361 purified by vacuum sublimation. BST was purchased from Luminescence Technology Corp. and all
362 other materials were purchased from Sigma-Aldrich and used as received.

363 *Device fabrication and measurement:* Hole-only devices were fabricated in a
364 glass/ITO/PEDOT:PSS(35 nm)/hole-transport layer/[interlayer]/metal oxide(10 nm)/Al(100 nm)
365 structure, in which the metal oxide was either MoO₃, WO₃, or V₂O₅. PEDOT:PSS was deposited by
366 spin coating and subsequent layers were thermally evaporated at a base pressures of $4-5 \times 10^{-7}$ mbar.
367 Symmetric devices were prepared in a glass/ITO/PEDOT:PSS/metal oxide/interlayer/hole-transport
368 layer/interlayer/metal oxide/Al structure. OLEDs were fabricated in a
369 glass/ITO/PEDOT:PSS/MoO₃/[C₆₀(4 nm)]/TPBi(58 nm)/Ba(5 nm)/Al(100 nm) structure. Electrical
370 characterization was carried out under N₂ atmosphere with a Keithley 2400 source meter, light output
371 was recorded with a calibrated Si photodiode, and electroluminescence spectra were obtained with a
372 USB4000-UV-VIS-ES spectrometer.

373 *UPS characterization:* UPS measurements were conducted at a base pressure of 10⁻⁹ mbar on Si/Cr(2
374 nm)/Au(50 nm)/MoO₃(10 nm)/organic substrates with a Kratos Axis Ultra^{DL} spectrometer (Kratos,
375 Manchester, England). During UPS measurement, the sample was held at a bias of -9 V with respect
376 to the spectrometer. Illumination at 21.22 eV was provided by the He(I) emission line from a helium
377 discharge lamp. Photoelectron emission was collected at 0° from the surface normal of the samples.
378 The spectra were taken in three different spots to confirm the spectra reproducibility and irradiation
379 exposure time was kept under one minute.

380 *Molecular simulations and density of states evaluation:* All morphology simulations were performed
381 using the GROMACS package and re-parametrized OPLS-AA force-field, as described in the
382 supplementary information. Density of states was evaluated using the VOTCA package [30,31] and
383 polarizable force-field (Thole model) as described in the Supplementary Information.

384
385 [29] Uoyama, H., Goushi, K., Shizu, K., Nomura, H. & Adachi, C. Highly efficient organic light-
386 emitting diodes from delayed fluorescence. *Nature* **492**, 234-238 (2012).

- 387 [30] Ruehle, V., Lukyanov, A., May, F., Schrader, M., Vehoff, T., Kirkpatrick, J., Baumeier, B. &
388 Andrienko, D. Microscopic simulations of charge transport in disordered organic
389 semiconductors. *J. Chem. Theory Comput.* **7**, 3335-3345 (2011).
- 390 [31] Poelking, C. & Andrienko, D. Long-range embedding of molecular ions and excitations in a
391 polarizable molecular environment. *J. Chem. Theory Comput.* **12**, 4516-4523 (2016).
- 392